*J. Fluid Mech.* (1979), *vol.* 90, *part* 3, *pp.* 569–588
*Printed in Great Britain*



# The mixing of rain with near-surface water

By T. GREEN AND D. F. HOUK†
Department of Civil and Environmental Engineering,
University of Wisconsin, Madison

(Received 27 October 1976 and in revised form 19 September 1977)

The mixing of rain with otherwise calm near-surface water is investigated experimentally, using both uniform drops and crude drop-size distributions. The results are interpreted in terms of mixed-layer depths and the upward entrainment of quiescent water. Large drops, even in quite small numbers, are shown to play a very important role in the mixing process. Entrainment coefficients vary as the inverse of a suitably defined bulk Richardson number, and behave similarly in both fresh and salt receiving water.

## 1. Introduction

The mixing of rain with near-surface water may be important both to air–sea interaction and climate research, because of the attendant change in water-surface temperature associated with near-surface dilution (Ostapoff, Tarbezev & Worthem 1972), and to studies of the biological character of near-surface water, because of the large associated changes in salinity and the introduction of foreign substances owing to washout (Mason 1971). In situations where the water is otherwise calm, significant dilution of the receiving water occurs at depths up to 30 cm; surface temperatures are changed as much as 5 °C. This naturally occurring mixing is a rather well-defined turbulent process, and can be investigated using conceptual tools devised in the course of previous mixing studies.

Even the interaction of a single drop with a quiescent receiving fluid is not simple. The associated Rayleigh jets, vortex rings and splash drops have been the object of a number of investigations (e.g. Levin & Hobbs 1971; Chapman & Critchlow 1967; Worthington & Cole 1897). When independent waves are present the process is more involved (Siscoe & Levin 1971). When many drops of varying size hit the fluid in a random manner, the situation is made far more complex by the interactions among various events and the effect of the associated underwater turbulence on any one event. However, the process is then spatially homogeneous in an average sense, so that certain integral aspects can be quite readily measured, and interpreted in the light of earlier, more controlled experiments on turbulent mixing. Exploratory measurements of rain mixing by Katsaros & Buettner (1969) have revealed the scales involved. Below we investigate some of the quantitative aspects of the process. Special attention is paid to the case of warm rain falling on cold fresh water.

There are certain advantages related to a laboratory experiment on rain mixing. There is no difficult scaling problem when comparing the results with natural processes: the laboratory scale is the natural scale. Also, the energy flux to the receiving water

† Present address: West Shore Community College, Ludington, Michigan.

is quite closely known. These two characteristics rarely hold in experiments using wind or an oscillating grid as the mixing agent. However, the process is so complex in other ways that some major simplifications are necessary. In our work, rain intensities were always constant in time and the drops were usually of uniform size. Wind and independent surface waves were absent. Until we understand the resulting rather simple situation, there is scant hope for coming to grips with more realistic cases.

## 2. Equipment and procedures

### 2.1. *Modelling rainfall*

Most rain research is carried out using rain modules (water-filled boxes with holes in the bottom) in which hypodermic needles generate known drop-size spectra. Such modules were used in the present work. The raindrop diameters depend on the needle size. The rain intensity is varied by changing the head of water in the module.

Three rain modules made of $\frac{1}{4}$ in. Plexiglas gave drop diameters of 2·2, 3·6 and 5·5 mm. Each module is 15 cm deep and 64·5 cm square. The 2·2 and 3·6 mm drops form at the end of 27- and 18-gauge needles. Nylon tubes $\frac{1}{4}$ in. in diameter were used to form the 5·5 mm drops; 20-gauge needles were inserted in the tubes to control the flow of water. The needles and tubes were placed in triangular formations (Mutchler 1965), 2·4 cm apart for the 2·2 and 3·6 mm drops and 3 cm apart for the 5·5 mm drops. Drops less than 1·5 mm in diameter were obtained by dropping 2·2 mm drops through a fine-mesh screen.

Modules were also constructed to give three drop sizes at the same time, to approximate natural rain with intensities of about 1·25 and 2·5 cm/h. The raindrop distribution for the former intensity consisted of 2 % of 5·5 mm drops, 13 % of 3·6 mm drops and 85 % of 2·2 mm drops. The distribution for the latter intensity consisted of 4 % of 5·5 mm drops, 23 % of 3·6 mm drops and 73 % of 2·2 mm drops. These modelled the natural distributions given by Laws & Parsons (1943).

Drop sizes were determined by allowing five drops to fall into a previously weighed beaker of olive oil. The drops settled to the bottom and did not evaporate. The beaker was then weighed again, the difference being the weight of the drops. The diameters $d$ were calculated assuming that the drops were spherical, although this is not precisely true (Mutchler 1967).

### 2.2. *The receiving tank and sensors*

The experiments took place in a vertical shaft with dimensions $3 \times 6 \times 16$ m. The supporting equipment was set up in rooms leading off the top and bottom of the shaft. A rain module was placed 14 m above a receiving tank (figure 1). The tank bottom and three of the walls were $\frac{3}{4}$ in. marine plywood. The fourth wall was $\frac{1}{4}$ in. glass. One inch of styrofoam insulation was placed on the inside walls and bottom. Tap water was used in both the receiving tank and the module. Air currents in the shaft were negligible. All drops were within 1 % of their terminal velocity when they hit the water. The temperature of the water in the tank was monitored with thermopiles, a thermistor and a radiation thermometer. The equipment and results discussed below are described in much more detail by Houk (1975), which is often referenced implicitly when results are described in the present paper.

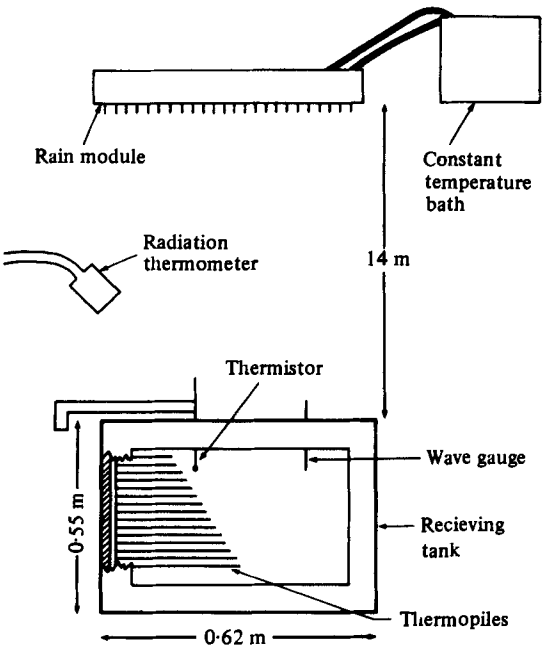


FIGURE 1. Schematic diagram of the experiment (not to scale).

A probe with 22 thermopiles measured the vertical temperature profile in the receiving tank. These data formed the primary basis for the results discussed below. Each thermopile consisted of four junctions in series, made from copper–constantan wire 0·01 in. in diameter. Each was separated in the vertical by 2 cm, was at an angle of 20° to those above and below, and was 1 cm longer than the thermopile just above it. The time constant was somewhat less than 1 s. Ice water served as the constant-temperature source. The probe floated upwards as rainwater was added to the tank, so that the top thermopile was always 5 mm under the water surface. Twelve thermopile temperatures were recorded on one Leeds & Northrup Speedomax H strip-chart recorder and the remaining ten on another. The sampling rate is one channel each 1·2 s, so that each thermopile was sampled every 14·4 s. The temperature profiles at 14·4 s intervals were obtained by digitizing the strip-chart output and converting to temperature via the individual thermopile calibrations. Temperatures were accurate to $\pm 0{\cdot}05$ °C.

The vertical temperature profile in the receiving tank was also measured occasionally with a Fenwall thermistor (type GB42SMM1) with a time constant of 0·07 s. This was mounted on a vertical rod, which moved up and down at any desired horizontal position. The velocity of the rod was 1·1 cm/s; the thermistor moved 0·08 cm during one time constant. The temperature and depth were recorded on a Clevite Mark 220 strip-chart recorder. Vertical temperature profiles were obtained by digitizing the thermistor output at 0·5 cm depth intervals and converting to temperature to an accuracy of $\pm 0{\cdot}05$ °C.

The temperature of the water in the top 10–100 $\mu$m was monitored by a radiation thermometer operating in the infrared region (8–14 $\mu$m). Either a Barnes PRT-6 or a Barnes IT-3 radiometer (with a sensitivity of 0·1 or 0·3 °C) was mounted 1·5 m

| Drop size (mm) | Intensity (cm/h) | Air temperature | Air wet-bulb temperature | Initial surface water temperature | Bottom water temperature |
|---|---|---|---|---|---|
| ⩽ 1·5 | 0·40 | 23·1 | 16·7 | 9·75 | 6·25 |
| | 0·50 | 23·1 | 16·7 | 8·75 | 6·40 |
| | 0·80 | 23·1 | 16·7 | 9·10 | 6·60 |
| | 0·90 | 23·1 | 16·7 | 15·30 | 13·90 |
| | 0·35 | 23·7 | 16·5 | 15·30 | 13·70 |
| | 0·90 | 23·7 | 16·5 | 15·35 | 13·90 |
| | 0·60 | 23·7 | 16·5 | 21·15 | 21·90 |
| | 0·50 | 23·7 | 16·5 | 19·30 | 19·90 |
| 2·2 | 0·60 | 22·7 | 16·5 | 8·95 | 6·15 |
| | 1·20 | 22·7 | 16·5 | 8·90 | 6·50 |
| | 1·80 | 22·7 | 16·3 | 9·00 | 6·18 |
| | 1·80 | 22·7 | 16·3 | 12·40 | 10·60 |
| | 1·10 | 23·0 | 15·5 | 11·40 | 10·00 |
| | 1·45 | 24·0 | 15·7 | 11·85 | 10·20 |
| | 1·40 | 24·0 | 15·8 | 12·50 | 10·80 |
| | 1·10 | 24·0 | 15·8 | 10·15 | 8·95 |
| | 0·50 | 23·9 | 18·0 | 16·40 | 15·40 |
| | 1·60 | 25·0 | 17·8 | 16·10 | 15·30 |
| | 0·20 | 25·0 | 17·8 | 18·90 | 19·10 |
| | 1·20 | 25·0 | 17·8 | 18·95 | 19·15 |
| 3·6 | 0·30 | 23·5 | 15·0 | 7·60 | 6·35 |
| | 1·45 | 23·9 | 17·5 | 13·25 | 11·25 |
| | 2·45 | 23·9 | 17·5 | 12·95 | 11·40 |
| | 3·45 | 23·9 | 17·5 | 13·35 | 11·50 |
| | 2·20 | 23·3 | 16·7 | 8·95 | 6·25 |
| | 1·60 | 23·3 | 16·7 | 8·05 | 6·60 |
| | 3·70 | 23·3 | 16·7 | 9·30 | 6·60 |
| | 1·85 | 23·2 | 17·2 | 15·80 | 14·35 |
| | 3·50 | 24·3 | 17·8 | 19·70 | 20·00 |
| | 2·90 | 24·3 | 17·8 | 21·50 | 21·85 |
| 5·5 | 0·70 | 23·5 | 16·7 | 9·40 | 6·20 |
| | 1·20 | 23·8 | 17·0 | 9·30 | 6·20 |
| | 2·30 | 23·8 | 17·0 | 9·50 | 6·60 |
| | 2·20 | 23·8 | 17·0 | 12·70 | 11·45 |
| | 0·40 | 23·3 | 16·0 | 12·00 | 10·75 |
| | 1·10 | 23·3 | 16·0 | 12·85 | 10·50 |
| | 1·15 | 23·3 | 16·0 | 13·00 | 10·75 |
| | 1·40 | 23·3 | 16·0 | 15·10 | 13·55 |
| | 0·30 | 22·8 | 15·0 | 14·40 | 12·70 |
| | 2·10 | 22·8 | 15·5 | 16·95 | 17·60 |
| | 0·90 | 22·8 | 15·5 | 16·90 | 17·45 |
| Variable | 1·20 | 23·9 | 17·4 | 10·25 | 6·85 |
| | 1·30 | 23·9 | 17·4 | 13·75 | 11·40 |
| | 1·40 | 23·9 | 17·4 | 16·45 | 15·40 |
| | 1·40 | 23·9 | 17·4 | 19·00 | 19·50 |
| | 2·00 | 23·9 | 17·5 | 21·10 | 21·60 |
| | 2·10 | 23·9 | 17·5 | 12·50 | 7·65 |
| | 2·55 | 23·9 | 17·5 | 13·10 | 11·85 |
| | 2·40 | 23·9 | 17·5 | 15·95 | 14·35 |

TABLE 1. Conditions for the freshwater rain experiments.
All temperatures are in °C.

above the tank and directed at an angle of 11° from the vertical. The temperature thus measured will be called the surface temperature $T_S$ below. This temperature was recorded on either a Speedomax H or a Gould 816 brush recorder, and was accurate to at least 0·3 °C. The data on the Speedomax H were digitized at 14·4 s intervals; those on the Gould were digitized at 5 min intervals.

The temperature of rain falling through a deep layer of air will reach and remain at the air wet-bulb temperature (Kinzer & Gunn 1951). The wet-bulb temperature of the air in the shaft was uniform. The water in the rain module was kept within 0·25 °C of this temperature by a Haake FK2 constant-temperature bath. Thus the temperature of the rain when it hit the surface water in the tank below was known to the same accuracy.

The rain intensity was monitored in two ways. A plastic ruler was glued to the side of the receiving tank and the increase in height of the water surface measured visually to the nearest 2 mm. A low-pass capacitance wave gauge was also used. The voltage output from the gauge was recorded on a Speedomax H. The digitized output gave the surface height to within $\pm$ 0·4 mm every 14·4 s.

The experimental set-up for salty receiving water was the same as that for fresh water, with the following exceptions. The rain intensities were measured only with the ruler, as the wave gauge corroded in salt water. The thermistor on the moving probe was replaced by a conductivity gauge to measure salinity.

### 2.3. *Procedures*

The first step in each experiment was to measure the temperature $T_A$ and the wet-bulb temperature $T_R$ of the air. A rain module was then placed above the receiving tank, and water from the constant-temperature bath set at $T_R$ was added to a depth corresponding to the desired rain intensity $I$. A plastic sheet underneath the module kept raindrops from falling into the receiving tank, which was meanwhile being filled with tap water. Ice was used to adjust the tank water temperature. The receiving tank was left undisturbed for 20 min. The plastic sheet was then removed to start the experiment. Recording of the outputs of the wave gauge, thermopile and radiation thermometer started 20 min before the rain began and continued for 5–10 min after the rain ended. Temperature profiles were usually taken with the thermistor at 5–10 min intervals. Forty-nine experiments were run; all but five lasted 1 h (table 1). The intensity $I$ ranged from 0·3 to 3·7 cm/h. The rain was between 13 °C warmer and 3 °C cooler than the water in the tank.

Seven salt-water experiments were run (table 6). Salinities were measured before the start of an experiment, at 5 min intervals up to 30 min, then every 10 min.

## 3. Rain falling into fresh water

The impact of warm water drops on a cold water surface creates a turbulent mixed layer (figure 2) which gradually deepens with time, mainly because of entrainment of the fairly quiescent fluid below the mixed layer. Internal waves exist on the thermocline (the lower boundary of the mixed layer) and capillary–gravity waves on the surface. The surface is also disfigured by Rayleigh jets associated with the rain (Siscoe & Levin 1971) and by the many splash drops due to raindrop impact, either directly, or indirectly by way of bursting bubbles or secondary splashes (Blanchard

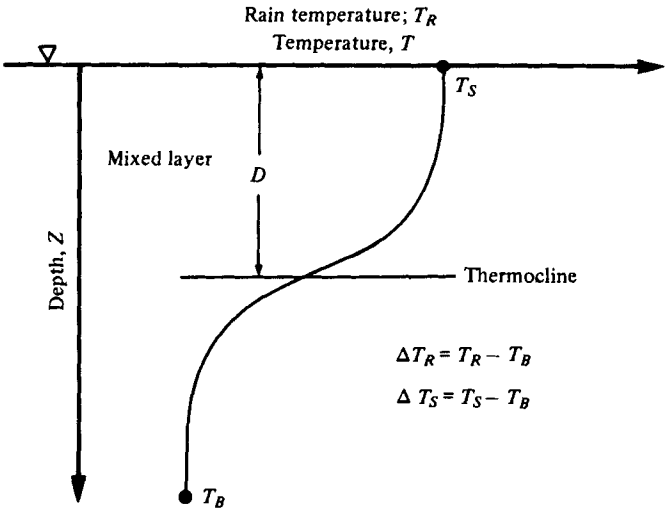


FIGURE 2. Nomenclature and symbols.

1966). Vortex rings associated with the Rayleigh jets are also present (Chapman & Critchlow 1967), and it is unclear how they or the waves interact with the mixed-layer turbulence. Most of these phenomena have been only studied quantitatively in the context of a single drop striking the water surface. Our aim was to study the integrated effects of all of the phenomena, and to deal with these effects in terms of entrainment and mixed-layer depth.

The thermocline will usually be taken to be at the depth $D$ where the vertical temperature variation is a maximum. All depth measurements $z$ given below are with respect to the water surface, which is moving slowly upwards because of the rain. Usually, however, the increase in $D$ with time is much greater than the rise in the surface. The temperature difference betseen the rain and the water at 42·5 cm (the depth of the bottom thermopile) is $\Delta T_R = T_R - T_B$. Similarly, $\Delta T_S = T_S - T_B$. Time $t$ is measured from the start of the rain. The symbols for the drop sizes used are: ●, smallest drops ($d < 1{\cdot}5$ mm); ○, 2·2 mm drops ($d = 2{\cdot}2$ mm); □, 3·6 mm drops; ×, 5·5 mm drops; *, variable drops ('Var' in the figures; $d = 2{\cdot}2$, 3·6 and 5·5 mm).

### 3.1. *Temperature profiles*

Figure 3 shows temperature profiles for some representative experiments. The profiles taken with the thermopiles are not simultaneous (see above). However, the temperature variations were small during a 14·4 s sampling interval, so that the measured profiles are very close to instantaneous profiles.

The water within 6 cm of the surface warms slightly in the 20 min period before the rain starts. The sensible heat flux from the air and the net long-wave radiation flux due to the warm shaft walls more than balance the cooling effect of evaporation at the surface. The heat is transferred downwards by molecular diffusion. This, of course, can also be the case just below a naturally occurring calm water surface. However, the departure from an isothermal state at $t = 0$ is unfortunate as it creates some interpretational difficulties.

The initial temperature profile is not changed in shape after the smallest (warm)

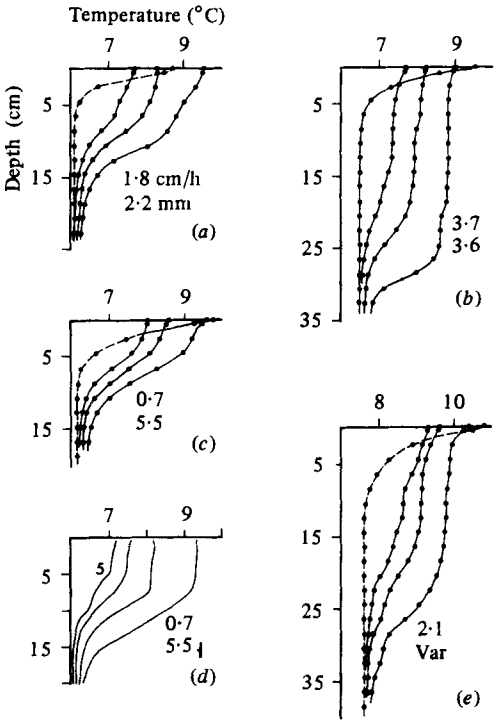


FIGURE 3. Representative temperature profiles: (*a*), (*b*), (*c*), (*e*) show thermocouple profiles at $t = 0$, 15, 30, 60 min; (*d*) shows thermistor profiles at $t = 5$, 15, 30, 60 min. The rain intensity (upper number) and drop size appear on each figure. The heat stored near the surface always increases with time.

raindrops start falling, and no definite thermocline forms. It is known that $T_S$ can vary by as much as 0·5 °C from the temperature below the first few tens of microns, so that the temperature recorded by a radiation thermometer may differ from that recorded by a thermistor barely immersed in the water (Saunders 1967). With the smallest drops, the molecular boundary layer at the surface remains intact: the surface temperature always remains 0·3–0·5 °C higher than the temperature measured by the top thermopile.

The warm 2·2 mm drops do form a thermocline. However mixing is not vigorous enough to produce uniform temperatures near the surface except in the case of large $I$ at small $\Delta T_R$. The surface temperature is always lowered after the rain begins. The boundary layer is now destroyed: after 5 min of rain, $T_S$ is always within 0·2 °C of the top thermopile temperature. Rain consisting of either 3·6, 5·5 mm or variable drops also breaks up the boundary layer: $T_S$ is always within $\pm$ 0·1 °C of the top thermopile temperature. At large $I$, the temperature is almost constant in the upper 15–30 cm after 15 min, owing to the mixing associated with the large raindrops.

Figure 3 also shows a typical temperature profile obtained with the thermistor. Inversions are often apparent in the thermistor profiles. They are probably associated with warm vortex rings propelled downwards from near the surface.

It would be satisfying to be able to describe the details of the mixing in a quantitative fashion. This is impossible without either turbulence measurements or extensive flow-visualization experiments. The thermocline shapes do give some clues (which are,

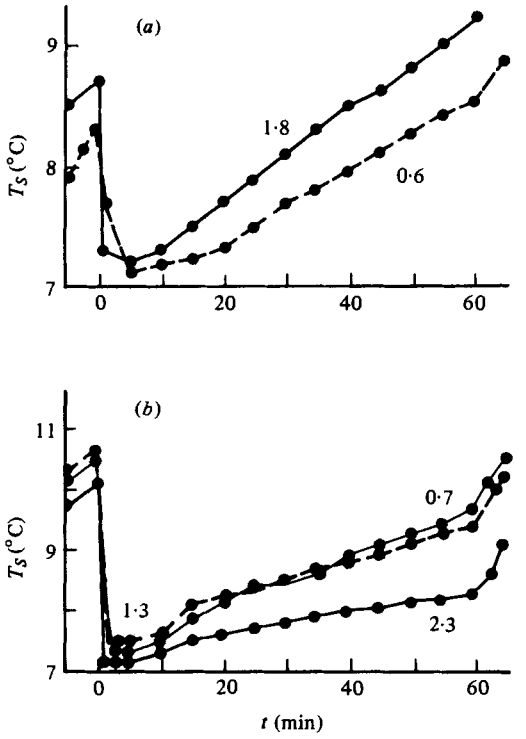


FIGURE 4. Typical surface-temperature variations with time: (*a*) $d = 2{\cdot}2$ mm, $I = 0{\cdot}6$ and 1·8 cm/h; (*b*) $d = 5{\cdot}5$ mm, $I = 0{\cdot}7$ and 2·3 cm/h; Var, $I = 1{\cdot}3$ cm/h. The curves for $I = 0{\cdot}7$ and 1·3 cm/h cross at $t \sim 20$ min; that for $I = 0{\cdot}7$ is higher for $t > 20$ min.

however, in accord with our intuition). In a given experiment, the maximum vertical temperature gradient $\delta$ increases with increasing $D$ (and $t$) because of the heat added to the upper layer and the relatively small effect of molecular heat diffusion near the surface. Also, for a fixed drop size, $\delta$ usually increases with increasing $I$ (and thus with increasing heat flux). The only exception was for small $I$ and $\Delta T_R$ and $d = 5{\cdot}5$ mm. In this case, $\delta$ was about 20 % larger for $d = 5{\cdot}5$ mm than for closely equivalent values of $I$ and $\Delta T_R$ for $d = 2{\cdot}2$ mm. The mixing due to the larger drops was clearly more vigorous, as expected. Other, similar comparisons showed a similar behaviour. Very small values of $\delta$ were found only for $D > 30$ cm. Below this level, molecular effects seem to dominate even for large $I$ and $d$, for warm rain falling into cold water.

The heat flux $Q_S$ through the water surface is due to that directly associated with the warm rain entering the water ($Q_R = \rho c_p I \Delta T_R$, where $\rho$ is the density and $c_p$ the specific heat), together with the warming or cooling of splash drops and the rough water surface by conduction and condensation or evaporation, and long-wave radiation. An attempt was made to separate $Q_S$ into these components. It was only partially successful, but suggested that splash-drop warming (in turn related to $d$ and $I$) contributes significantly to the total. In view of the tentative nature of the results, they will not be discussed here.

Typical surface temperature variations with time are shown in figure 4. $T_S$ drops sharply just after the rain begins owing to the heat in the surface layer being mixed over a deeper layer. After 5 min, $T_S$ starts to increase, owing mainly to the warming

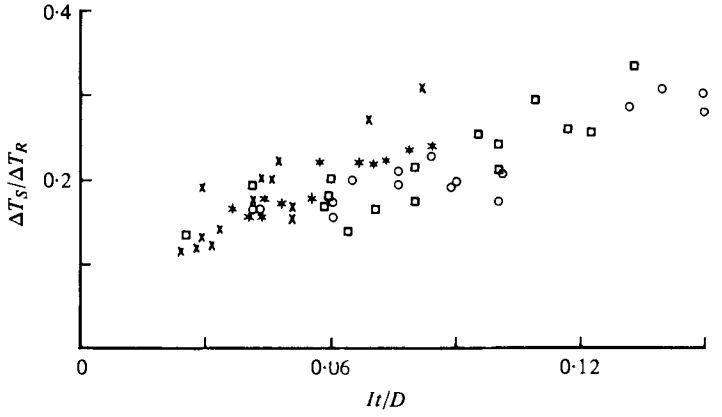


FIGURE 5. Normalized surface-temperature variations at $t = 30$ and 60 min.

of the near-surface water by the heat input of the rain. The ratio $\Delta T_S/\Delta T_R$ is shown to scale reasonably well with the non-dimensional quantity $It/D$ in figure 5, although there does seem to be a slight increase in this ratio with increasing drop size. The success of these dimensionless groupings is not especially surprising. If heat is conserved in the surface layer, i.e. $T = T_S$ throughout this layer, and $T = T_B$ (a constant) below the layer, then

$$D\frac{dT_S}{dt} + (T_S - T_B)\frac{dD}{dt} = \frac{d}{dt}(D\Delta T_S) = \frac{Q_S}{\rho c_p}.$$

Then if $Q_S = Q_R$, a constant,

$$D\Delta T_S = Q_R t/\rho c_p = I\Delta T_R t,$$

which leads directly to the dimensionless groupings in figure 5. Actually, $Q_S > Q_R$ as noted above, so that $\Delta T_R/\Delta T_S > It/D$, as shown in figure 5. This, plus the fact that $T \neq T_S$ in the surface layer (and that the temperature-profile shape changes with time), limits the above analysis to an argument, rather than an explanation, for the groupings used.

When cold rain fell into warm water the tank cooled off uniformly from top to bottom. Before the rain, $T_S$ was lower than the water temperature at the top thermopile. Again, the surface boundary layer was broken up by all but the smallest drops, and $T_S$ equalled the temperature at the top thermocouple. For the smallest drops, the cool surface layer persisted throughout the experiment. These experiments will not be discussed further.

### 3.2. *Thermocline irregularities*

The mixed layer was sometimes dyed, and photographs of the interface thus revealed taken. This interface was quite sharp and very close to the thermocline; no distinction could be made between the two. The shape was usually complicated and irregular; internal waves up to 1 cm in height existed. The Brunt–Väisälä period $2\pi/\{\alpha g|dT/dz|_I\}^{\frac{1}{2}}$ was calculated by using the thermal expansion coefficient $\alpha$ at the average interface temperature and taking $(dT/dz)_I$ as the average temperature gradient over 2 min, using the temperatures 2 cm above and below the mean interface depth ($g$ is gravity). The smallest period found was 58 s. Internal waves found by placing the thermistor at the thermocline had similar periods.

| Drop size (mm) | Intensity (cm/h) | Thermocline depth (cm) | Maximum calculated r.m.s. wave amplitude (cm) | Brunt–Väisälä period (s) |
|---|---|---|---|---|
| 2·2 | 0·6 | 6 | 1·1 | 89 |
| | 0·6 | 8 | 0·6 | 73 |
| | 1·8 | 6 | 1·5 | 87 |
| | 1·8 | 10 | 0·8 | 64 |
| 3·6 | 1·6 | 8 | 1·5 | 104 |
| | 1·6 | 14 | 0·9 | 67 |
| | 3·7 | 12 | 1·5 | 102 |
| | 3·7 | 28 | 1·0 | 87 |
| 5·5 | 0·7 | 6 | 1·0 | 73 |
| | 0·7 | 10 | 0·8 | 63 |
| | 2·3 | 28 | 2·0 | 125 |
| | 2·3 | 34 | 1·4 | 104 |
| Variable | 1·3 | 8 | 0·8 | 80 |
| | 1·3 | 14 | 0·7 | 73 |
| | 2·1 | 18 | 1·9 | 101 |
| | 2·1 | 26 | 1·0 | 89 |

TABLE 2. Calculated thermocline displacements due to internal waves, and Brunt–Väisälä periods (see text).

Wave amplitudes were estimated indirectly for several experiments. A linear least-squares fit was applied to temperatures for times up to 8 min, at the thermopile where the thermocline was located, to remove the long-term warming trend. The temperature deviations $T_I'$ from this fit were calculated over a 2 min interval, squared and averaged. The r.m.s. deviation of the interface $\eta$ was estimated from an equation valid for internal waves on a linearly varying density field (Deardorff, Willis & Lilly 1969):

$$\eta = (\overline{\Sigma T_I'^2})^{\frac{1}{2}} \Big/ \left(\frac{dT}{dz}\right)_I .$$

Some results are shown in table 2. The displacements are similar to those observed when the upper layer was dyed. Note that the displacements decrease with increasing thermocline depth, in accord with the energy input being at the surface.

### 3.3. *The depth of mixing*

The depth of the mixed layer is important in estimating surface-water dilution and surface temperature. Now $dT/dz$ is taken as $(T_1 - T_2)/(z_1 - z_2)$, where $T_1$, $T_2$ and $z_1$, $z_2$ are the temperatures and depths of adjacent thermopiles, and is calculated for all adjacent thermopiles for each 14·4 s interval. When $dT/dz$ over one interval exceeded its values at all other levels for at least 1 min (the Brunt–Väisälä period) the thermocline was taken to be at the midpoint of that interval. In a few experiments, the temperature sometimes decreased linearly over a distance greater than 2 cm. Here $D$ was taken to be the midpoint of the depth interval over which the maximum temperature gradients occur. Note that this definition of $D$ tends to remove the effect of molecular heat conduction. It may be better to define $D$ in terms of heat transfer through the surface and take to be at (say) the level above which 90 % of the heat transferred through the surface is stored. This heat-storage definition was also used for some

| Drop size (mm) | Intensity (cm/h) | $t = 10$ min $D_T$ | $t = 10$ min $D_H$ | $t = 40$ min $D_T$ | $t = 40$ min $D_H$ |
|---|---|---|---|---|---|
| 2·2 | 0·60 | 5·7 | 6·2 | 7·2 | 8·4 |
| | 1·80 | 8·0 | 8·5 | 11·0 | 11·2 |
| | 1·80 | 8·2 | 8·9 | 11·0 | 10·6 |
| 3·6 | 1·60 | 10·5 | 11·7 | 14·8 | 16·7 |
| | 3·70 | 15·3 | 15·3 | 25·0 | 24·7 |
| | 0·30 | 5·0 | 7·7 | 7·8 | 10·2 |
| 5·5 | 0·40 | 5·5 | 5·7 | 8·9 | 9·8 |
| | 1·20 | 13·5 | 13·9 | 27·0 | 27·5 |
| | 2.30 | 28·0 | 25·6 | 38·5 | 37·4 |
| Variable | 1·30 | 10·1 | 11·3 | 16·2 | 16·7 |
| | 2·10 | 19·7 | 18·8 | 26·0 | 25·5 |

TABLE 3. Comparison of mixed-layer depths (in cm) calculated from the heat storage ($D_H$) and from the maximum temperature gradient ($D_T$).

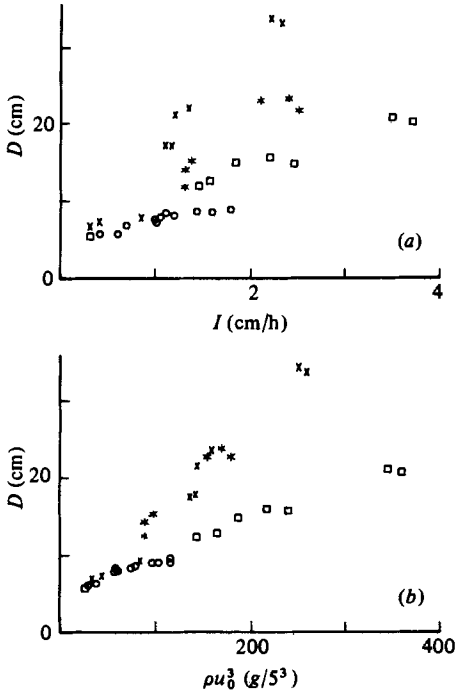


FIGURE 6. Mixed-layer depths after 20 min of rain.

experiments, and $D$ was found to vary little whether calculated using heat storage or $dT/dz$ (table 3). This suggests that molecular effects are small compared with the mechanical mixing due to the rain. As a final check, the thermistor profiles were also used to calculate $D$, using the criterion that $dT/dz$ be a maximum. The average value of the 'thermistor depth' minus the 'thermopile depth' was $-0{\cdot}3$ cm, with maximum deviations of $\pm 1{\cdot}2$ cm. The variations are probably caused by the internal waves discussed above.

Mixed-layer depths after 20 min are shown in figure 6. The influences of drop size and intensity are evident. The mixed layers caused by the variable drops show clearly the effect of large drops on mixing, even though they are small in number. The mixed layer should be strongly affected by the mechanical energy flux through the water surface $\kappa = \rho u_*^3 = \frac{1}{2}\rho I \times$ (raindrop terminal velocity)$^2$ (Houk & Green 1976). $D$ is also plotted against $\kappa$ in figure 6. The smaller and larger drop sizes now scale better, separately, although there is still a very noticeable dependence on drop size. The larger drops probably create much larger eddies which are more efficient in mixing buoyant water downwards. Moreover, the increased mixing tends to make the difference

$$\Delta\rho = \frac{1}{D}\int_0^D \rho\, dz - \rho_I$$

between the average density over the mixed layer and that at the thermocline smaller for the larger drops, thus giving a smaller resisting buoyancy and increasing $D$ at a fixed $\kappa$. The extent to which buoyancy affects the mixing will be discussed further below. Note that $\kappa$ is independent of rain buoyancy with respect to the receiving water. Finally, hexadeconal was added to the surface of the receiving water in some experiments, mainly to estimate its rate of removal by rain. This changed the surface tension by a factor of two, but had no noticeable effect on $D$.

The fraction $\epsilon$ of rainwater in the mixed layer can be estimated best using the heat-storage definition of $D$:

$$\epsilon = 0{\cdot}90 Q_S t/\rho c_p D\Delta T_R.$$

It is hard to estimate $Q_S$ in general (see above). For small drops, $Q_S \sim Q_R$ (see Houk 1975), so that $\epsilon \sim 0{\cdot}9It/D$. The prediction of $D(t)$ will be discussed below.

### 3.4. *Entrainment*

The descent of the thermocline owing to the upward entrainment of bottom fluid can be described by an entrainment coefficient $E$, the ratio of the descent rate $dD/dt$ to a characteristic velocity in the turbulent layer, taken here to be $u_*$. Other choices for characteristic velocity are discussed by Turner (1973, chap. 9). The descent rate was obtained by graphical differentiation. Because of the difficulty in accurately determining $D$, its derivative with respect to time is subject to some uncertainty.

The Reynolds number of the mixed layer $u_* D/\nu \sim 5000$, so that molecular processes should not influence the entrainment significantly (see, for example, Turner 1968). The initial temperature profiles shown in figure 3 suggest that molecular diffusion effects are at most 10–20 % of those due to mechanical mixing. In view of the large scatter in the results (typical of such mixing experiments), this molecular effect can be ignored as a first approximation. See also the other comments made above. Then $E \equiv u_*^{-1} dD/dt$ is a function of $g\Delta\rho/\rho$, $u_*$ and $D$ (which should characterize the scale of the turbulence in the region where rain mixing is significant), so that $E$ can be related to an overall Richardson number of the mixed layer:

$$E = E(Ri), \quad Ri = \frac{gD\Delta\rho}{\rho u_*^2}. \tag{1}$$

The use of $u_*$ as the velocity scale is, of course, open to question, especially for large $D$. It is the most reasonable first guess, and organized the results better than other choices (such as $I$). We return to this point later.

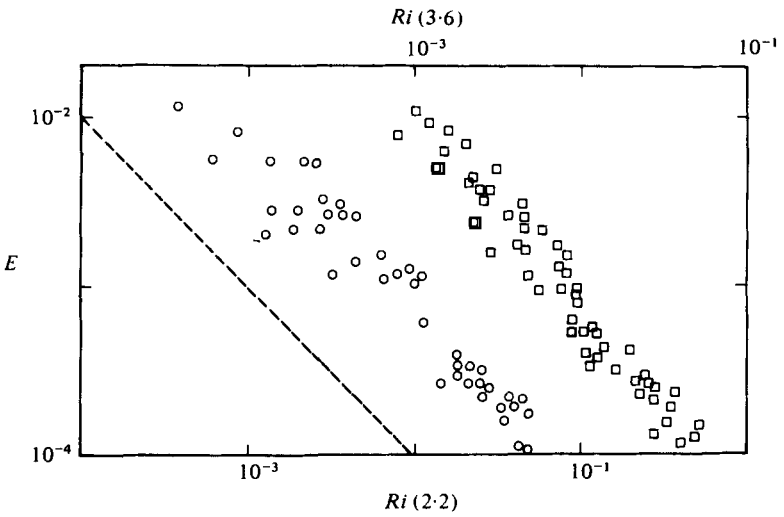


FIGURE 7. Entrainment coefficients against Richardson number for 2·2 and 3·6 mm drops. The dashed line has slope −1.

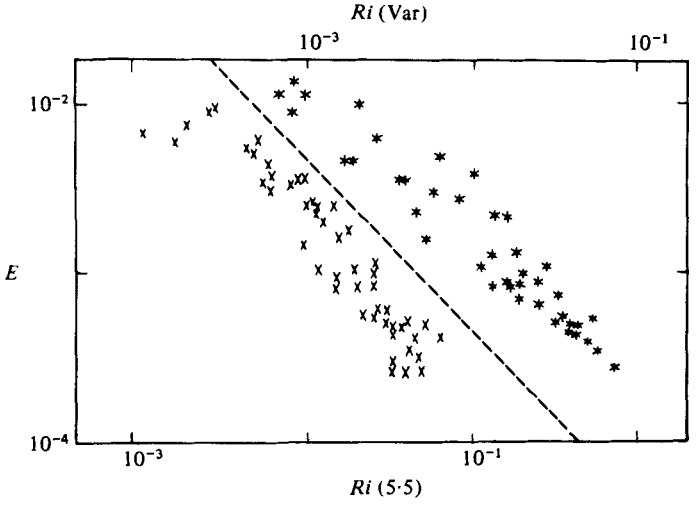


FIGURE 8. Entrainment coefficients against Richardson numbers for 5·5 mm and variable drops.

The data are plotted as $E(Ri)$ in figures 7 and 8. Although there is scatter similar to that in other laboratory mixing experiments, there does not seem to be a significant departure from (1). Linear least-squares fits to the data give slopes of −0·95, −0·97, −0·94 and −0·92 for the 2·2, 3·6, 5·5 mm and variable drops. Minus-one slopes fit individual experiments better than the aggregate at any one drop size, indicating the presence of secondary (and unknown) scaling parameters, perhaps associated with molecular processes. We assume the slope to be −1 for each drop size, and calculate the average value of $\lambda$ in the equation $E = \lambda/Ri$ and its standard deviation $\sigma$ for each raindrop size (see table 4). The variations reflected in $\sigma$ are probably due mainly to difficulties in calculating $dD/dt$, but also point to the existence of secondary factors.

| $d$ | $\lambda \times 10^6$ | $\sigma \times 10^6$ |
|---|---|---|
| 2·2 mm | 8 | 3 |
| 3·6 mm | 8 | 3 |
| 5·5 mm | 18 | 6 |
| Variable | 16 | 6 |

TABLE 4

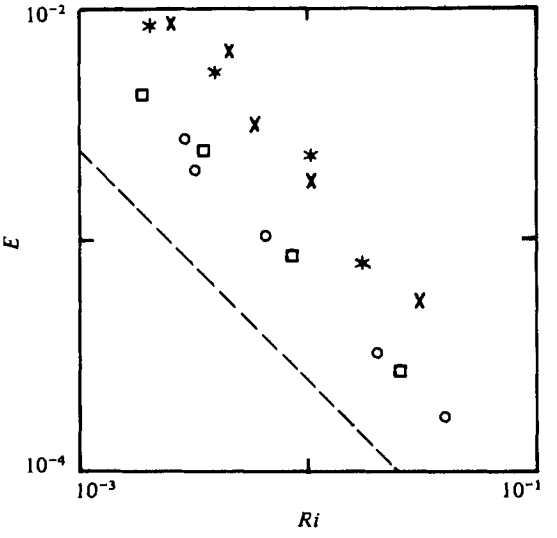


FIGURE 9. Entrainment coefficients against Richardson numbers for four typical experiments Here the heat-storage definition of $D$ was used to calculate $Ri$.

The entrainment is much larger for the 5·5 mm and variable drops (recall figure 6). This difference may be explained by the fact that $u_*$ is defined in terms of the external kinetic energy input. The deepening of the mixed layer should depend on the turbulent velocity and length scales near the interface. Although we could not find a reasonable correction factor from our limited data, it seems likely that for the 2·2 and 3·6 mm drops $u_*$ overestimates the interface velocity scale. The entrainment for variable drops shows the great influence of the 5·5 mm drops, even though they constitute less than 5 % of the total rain volume.

$E$ was also calculated with $D$ defined by heat storage (figure 9). The best-fit slopes now range from $-0{\cdot}98$ for the variable drops to $-1{\cdot}06$ for the 2·2 mm drops. These slopes are closer to minus one, and reflect the fact that fewer experiments were used, in accord with the statements above regarding secondary parameters. The slopes of the $E(Ri)$ curves are again assumed to be $-1$, and the constants are given in table 5. All of the constants are within 20 % of those given previously; the $E(Ri)$ relations are pleasantly insensitive to the definition of $D$.

| $d$ | $\lambda \times 10^6$ |
|---|---|
| 2·2 mm | 7 |
| 3·6 mm | 8 |
| 5·5 mm | 19 |
| Variable | 18 |

TABLE 5

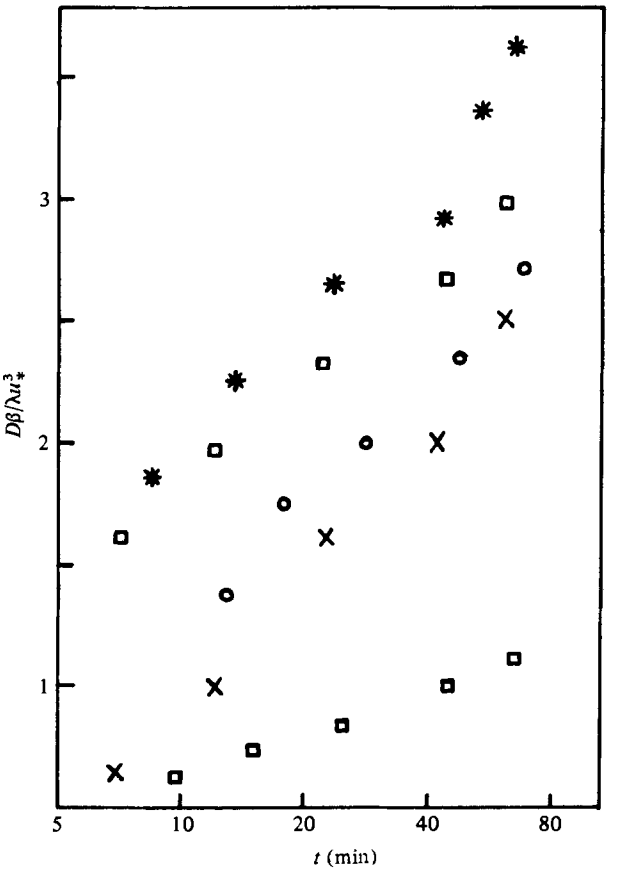


FIGURE 10. Normalized depth $D\beta/\lambda u_*^3$ *vs.* time for the experiments with ($d$, $I$) values of (2·2, 1·60), (3·6, 0·30), (3·6, 1·85), (5·5, 1·20) and (Var, 2·55), in cgs units. The logarithmic behaviour of $D(t)$ is in accord with (2). The Var results for $D$ have been halved for convenience in plotting.

### 3.5. *Predicting the mixed-layer depth*

Although the entrainment coefficients discussed above are the most fundamental part of this work, there is some interest in using the data to predict the mixed-layer depth. Such a prediction, however, may not be especially useful. For example, our ignorance of the heat transfer due to splash drops implies that the buoyancy flux in field conditions will not be accurately known.

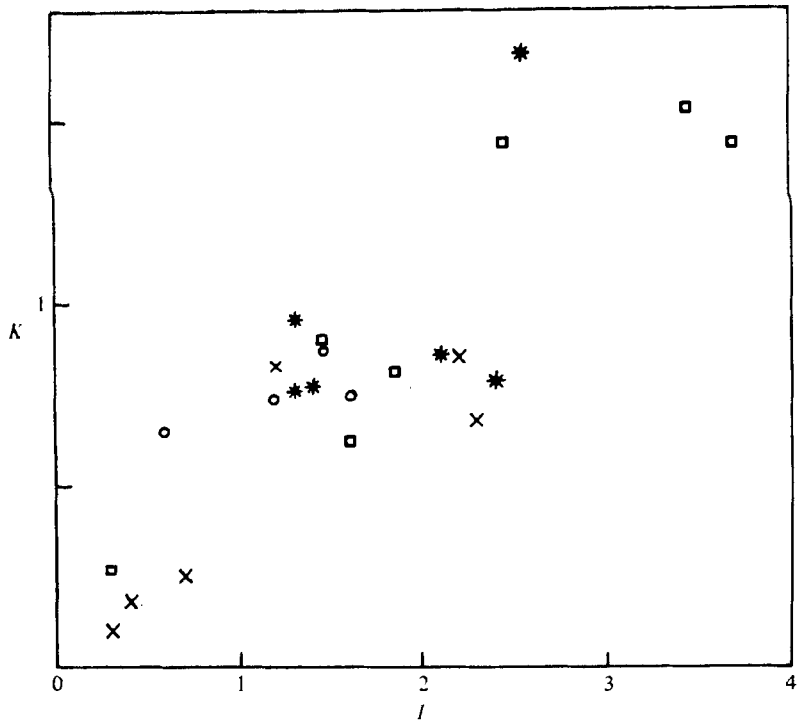


FIGURE 11. The constant $K$ in (2) *vs.* the rain intensity $I$. Each point represents the best-fit value for an individual experiment.

Assuming (admittedly roughly) that $\Delta\rho = \rho_S - \rho_B = \alpha\rho\Delta T_S$ and using the fact that $\Delta T_S/\Delta T_R \propto It/D$ (figure 5), the entrainment relation $E = \lambda/Ri$ implies

$$tdD/dt \propto \lambda u_*^3/\beta_R,$$

where $\beta_R = \alpha g Q_R/\rho c_p$ is the buoyancy flux directly associated with the rain. Then

$$D = K\frac{u_*^3}{\beta_R}\ln(t/\tau), \tag{2}$$

where $\tau$ is a time scale for the mixing process and $K$ a constant containing both $\lambda$ and a proportionality constant for the relation given just above.

The experimental values $D(t)$ do show a pronounced logarithmic behaviour (figure 10). The (best-fit) values of $K$ for individual experiments generally increase with $I$ (figure 11), but show little correlation with drop size or buoyancy flux. The values of $\tau$ range from 1 to 3 min, but show no correlation with physical parameters.

The scatter and lack of correlation are, of course, unsettling. A major problem was very likely the surface warming before the rain began (e.g. figure 3). We tried to correct for this by extrapolating the total heat added to the receiving water backwards to find a new, fictitious starting time for each experiment. This gave the $K$ and $\tau$ values shown, and did reduce the scatter somewhat. That remaining probably reflects the crudeness of this correction, the fact that the initial mixing may well be governed by a different, impact-type, physical process, the splash-drop warming discussed above, and the validity of assumptions such as $\Delta\rho = \rho_S - \rho_B$. This is a long list. Thus the usefulness of (2) is questionable, although it may be a first approximation.

| Drop size (mm) | Intensity (cm/h) | Air temperature | Air wet-bulb temperature | Bottom water temperature | Initial salinity (‰) |
|---|---|---|---|---|---|
| ⩽ 1·5 | 0·1 | 24·0 | 18·4 | 20·25 | 30·0 |
| 2·2 | 0·4 | 24·0 | 19·0 | 20·30 | 30·9 |
| | 0·9 | 24·3 | 18·2 | 22·25 | 30·4 |
| 3·6 | 1·6 | 24·3 | 18·2 | 22·00 | 31·2 |
| | 3·3 | 24·0 | 19·0 | 20·25 | 29·2 |
| 5·5 | 1·0 | 24·5 | 17·8 | 20·50 | 33·7 |
| Variable | 1·9 | 24·5 | 17·8 | 20·70 | 33·0 |

TABLE 6. Conditions for the saltwater rain experiments. All temperatures are in °C.

### 3.6. *Mechanical energy flux*

In this experiment, we know quite closely the flux of mechanical energy $\kappa$ through the water surface and can thus estimate the mechanical energy budget for the water column. The rate of increase of potential energy over that obtained by simply adding the rain to the water surface (i.e. by having no mixing) is easily calculated from the temperature profiles. It is found to be at most $3 \times 10^{-4}\kappa$. Wu (1973), in a similar calculation of the potential energy flux associated with the descent of the mixed layer owing to surface wind, found a value of about 0·25 % of the energy input from the wind. The flux of energy to surface waves is estimated by assuming a steady state and measuring the wave decay immediately after stopping the rain. This was done for the variable drops, and gave a flux of about $2 \times 10^{-2}\kappa$. Similar calculations for internal waves gave $10^{-5}\kappa$. Thus it seems that the vast majority of $\kappa$ goes directly into either subsurface turbulence or organized motions such as vortex rings. The above are, of course, integral estimates, and sidestep questions such as that regarding energy transfer between surface waves and turbulence.

## 4. Rain falling into salt water

In order to estimate the relevance of the above work to the ocean, rain was allowed to fall into water of various salinities $S$ between 29 and 34‰ in a small number of experiments (table 6). Salinity profiles were obtained by digitizing the raw data at 0·1 cm depth intervals and converting to salinity to within 0·01‰. The mixed layer was now bounded from below by both a thermocline and a halocline. The halocline was usually much sharper than the thermocline, owing presumably to the large difference between thermal conductivity and salt diffusivity. Many of the results are parallel to those discussed above, and will receive little attention below.

Figure 12 shows the variation of surface salinity and temperature with $It/D$. It should be noted that the sea surface temperature will vary significantly from the bulk temperature after 15 min of rain on calm water.

The mixed layer is now defined by the halocline, because the much slower increase in $D$ with time in salt water made necessary the increased resolution possible using the moving conductivity gauge. The value of $D$ found using the maximum value of $dS/dz$ always differed by less than 0·5 cm from that calculated from a 'freshwater-

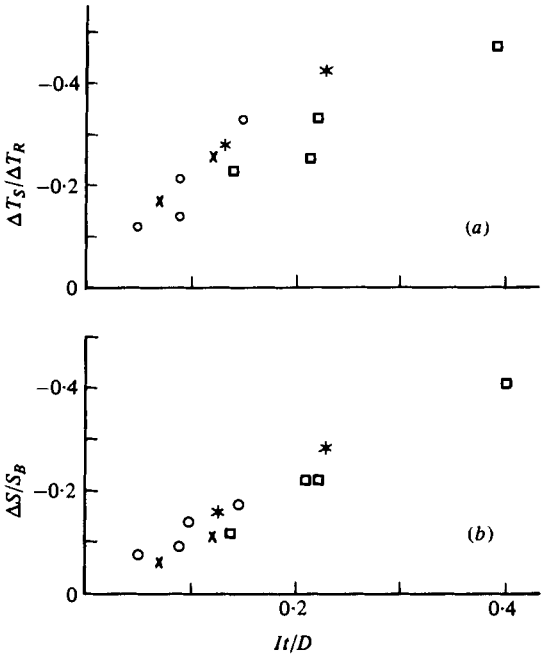


FIGURE 12. Normalized surface temperatures and salinities at $t = 30$ and 60 min.

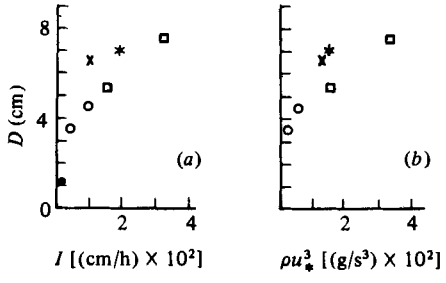


FIGURE 13. Mixed-layer depths in salt water after 20 min of rain.

storage' definition analogous to the heat-storage definition above. The mixed-layer depths after 20 min are shown in figure 13. The influence of drop size is not as striking as in the freshwater experiments, although the variable-drop results again show clearly the large effect of a small fraction of large drops. The mixed-layer depths are only about a third of those in freshwater for similar $d$ and $I$, because of the much larger buoyancy fluxes. It appears that we can still neglect molecular processes with some confidence, because of the extremely small diffusivity of salt.

The descent of the interface is interpreted in terms of entrainment in figure 14. To find $\rho(z)$ at 1 mm intervals, temperatures were linearly interpolated between adjacent thermopiles and Eckart's (1958) equation of state used. The values of $\lambda = E\,Ri$ are given in table 7. They are larger than the corresponding constants for the freshwater experiments, although within one standard deviation of those constants.

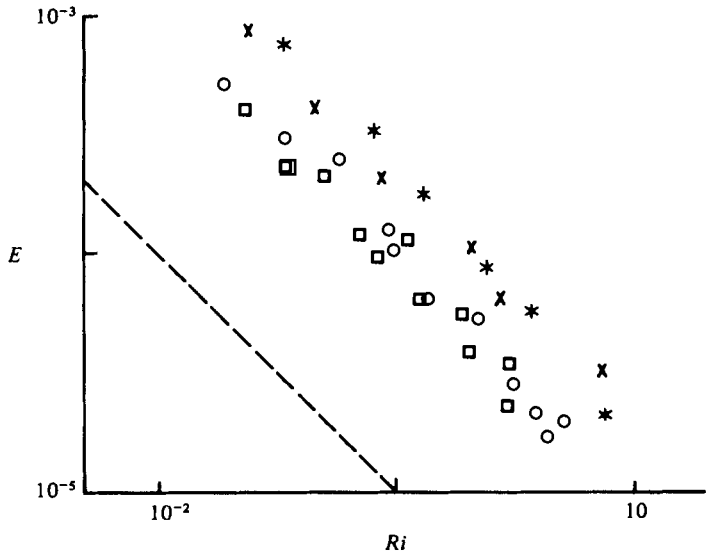


FIGURE 14. Entrainment coefficients against Richardson numbers for salt water.

| $d$ | $\lambda \times 10^6$ | $\sigma \times 10^6$ |
|---|---|---|
| 2·2 mm | 10 | 2 |
| 3·6 mm | 9 | 2 |
| 5·5 mm | 20 | 3 |
| Variable | 22 | 5 |

TABLE 7

## 5. Summary

Our experiments were aimed at eliciting the overall effects of a large number of raindrops striking a water surface randomly at their terminal velocity. We have shown that there is some order in the mixing process. The entrainment coefficients quite clearly vary inversely with the bulk Richardson number, although the variation of the constant $\lambda$ with drop size suggests that $u_*$ and $D$ may not be the most suitable scales for velocity and length near the interface, at least over a wide range of drop sizes.

A foundation has been presented for predicting the depth of the mixed layer due to rain buoyant with respect to the receiving water. Such a prediction would also allow a calculation of rainwater dilution in otherwise calm conditions. However, the method depends upon knowing the values of $K$ and $\tau$, which have yet to be clearly related to physical quantities, probably because of the various experimental difficulties noted in § 3 above.

It should be noted that the entrainment relations $E(Ri)$ depend only on knowing $\Delta\rho$, and thus do not depend upon understanding the mechanics of surface heat transfer. They are also quite insensitive to the precise definition of the mixed-layer depth $D$. These relations are probably the major contribution of our work.

Because of the complexity of the process studied, it is not surprising that many questions remain. That most germane to our work concerns the above-mentioned variation of $\lambda$ with $d$. This question must be resolved before the mixing effect of a continuously varying drop-size distribution can be ascertained. The use of $D$ and $u_*$ as the only length and velocity scales is clearly rather dubious, and should be explored carefully in further work. The relation of the rain-induced turbulence to $I$, $d$ and $\Delta T_R$, together with its decay with depth, would yield much relevant information. Detailed flow-visualization studies might also be quite useful. A thorough sorting out of all the individual mixing processes enumerated at the beginning of § 3 is needed for a full understanding of the process studied. However, their interactions may well be so complex that this sorting out will be some time in coming. It is likely that only then will one be able to come to grips with the important question of the relation of rain to the small-scale action of wind on a water surface.

## REFERENCES


CHAPMAN, D. S. & CRITCHLOW, P. R. 1967 *J. Fluid Mech.* **29**, 177.

DEARDORFF, J. W., WILLIS, G. E. & LILLY, D. K. 1969 *J. Fluid Mech.* **35**, 7.

ECKART, C. 1958 *Am. J. Sci.* **256**, 225.

HOUK, D. F. 1975 Ph.D. dissertation, The University of Wisconsin.

HOUK, D. F. & GREEN, T. 1976 *J. Geophys. Res.* **81**, 4482.

KATSAROS, K. & BUETTNER, K. J. K. 1969 *J. Appl. Met.* **8**, 15.

KINZER, G. D. & GUNN, R. 1951 *J. Met.* **8**, 71.

LAWS, J. O. & PARSONS, D. A. 1943 *Trans. Am. Geophys. Un.* **24**, 452.

LEVIN, Z. & HOBBS, P. V. 1971 *Phil. Trans. Roy. Soc.* A **269**, 555.

MASON, B. J. 1971 *The Physics of Clouds.* Oxford: Clarendon Press.

MUTCHLER, C. K. 1965 *J. Geophys. Res.* **70**, 3899.

MUTCHLER, C. K. 1967 *J. Soil Water Conservation* **10**, 91.

OSTAPOFF, F., TARBEZEV, Y. & WORTHEM, S. 1972 *Science* **180**, 960.

SAUNDERS, P. M. 1967 *J. Atmos. Sci.* **24**, 269.

SISCOE, G. L. & LEVIN, Z. 1971 *J. Geophys. Res.* **76**, 5112.

TURNER, J. S. 1968 *J. Fluid Mech.* **33**, 639.

TURNER, J. S. 1973 *Buoyancy Effects in Fluids.* Cambridge University Press.

WORTHINGTON, A. M. & COLE, R. S. 1897 *Phil. Trans. Roy. Soc.* A **180**, 137.

WU, J. 1973 *J. Fluid Mech.* **61**, 275.